# Spatially Decoupling of CP Antennas Based on FSS for 30-GHz MIMO Systems

**MOHAMMAD AKBARI**[1]**, (Student Member, IEEE),**
**HAMDAN ABO GHALYON**[1]**, (Student Member, IEEE),**
**MOHAMMADMAHDI FARAHANI**[2]**, (Student Member, IEEE),**
**ABDEL-RAZIK SEBAK**[1]**, (Fellow, IEEE),**
**AND TAYEB A. DENIDNI**[2]**, (Senior Member, IEEE)**
[1]Department of Electrical and Computer Engineering, Concordia University, Montréal, QC H3G2W1, Canada
[2]Institut National De La Recherche Scientifique, Montréal, QC H5A1C6, Canada

Corresponding author: Mohammad Akbari (akbari.telecom@gmail.com)

**ABSTRACT** In this paper, an effective approach for mitigating the near-field coupling between four-port circularly polarized (CP) antennas in a 30-GHz multiple-input, multiple-output (MIMO) system is suggested and investigated. This is obtained by incorporating a two-layer transmission-type frequency selective surface (FSS) superstrate based on planar crossed-dipole metal strips. This paper presents a comparison between the mutual coupling when the patches are radiating in free space and in the presence of the FSS layers. The simulated results, when the FSS layers are applied, show an average of 6–12-dB improvement in the isolation between four adjacent CP-MIMO antennas. In addition, an accurate study is carried out on the insignificant reflections produced by the FSS layers to redirect those and also prevent any interference. The proposed $2\times2$ CP-MIMO antenna along with the superstrate is implemented and tested to validate the simulation results. Experimental results of the coupling and reflection coefficients and axial ratio show an acceptable agreement with the corresponding simulated ones.

**INDEX TERMS** MIMO, coupling reduction, frequency selective surface (FSS), cross dipole, circularly polarized (CP), antenna.

## I. INTRODUCTION

Mutual coupling refers to the interactions between electromagnetic fields of the adjacent antenna elements. It can degrade the antenna array performance in terms of impedance and radiation characteristics [1]. Depending on the shape of antennas (i.e., planar or nonplanar), fabrication technologies, arrangement type, and distance between them, mutual couplings are categorized as follow: (i) the signal leakage via surface wave propagating along substrate dielectric and air interface [2], [3], (ii) the conducting current due to the existence of continuous metallic ground plane [4], (iii) the mutual coupling between the feeding lines [5], and (iv) the coupling due to the spatial electromagnetic fields [6]. Multiple-input multiple output (MIMO) systems in millimeter-wave (MMW) frequency band have become an emerging technology for future indoor and outdoor communications because they permit the next generation mobile networks (NGMN) to provide high data rates in order to improve the link performance [7]. Improvement in throughput and

radiation efficiency of MIMO wireless systems demands a lower envelope correlation and further degree of isolation between the adjacent antennas [8]. Therefore, mutual coupling reduction between closely spaced antennas in MIMO systems has been studied by various authors [9]–[10]. Mutual coupling affects the MIMO system performance through varying the impedance and radiation characteristics, which degrades the side-lobe level and radiation pattern shape [9]. In order to increase the signal-to-noise ratio and enhance the channel capacity of MIMO systems, the inter-element spacing should be minimum (a half wavelength) [9]. However, the space left for antenna elements and fabrication restrictions are usually heavily restricted in the highly integrated wireless communication systems. One should note that such a limited inter-element spacing results in a strong mutual coupling, radiation efficiency reduction, and functional deterioration of the system [6]. Isolation approaches are extensively reported in the literature to reduce mutual coupling effects [2]-[20]. Lumped elements connected in shunt are adjusted to decouple

the isolation between two adjacent patch antennas [11]-[12]. At low-frequency 2.45GHz, a new narrow-band decoupling technique has been proposed with a considerable compact decoupling network [11]. It is an effective technique for coupling reduction but typically results in a narrow-band behavior and is considered as a complex structure to be utilized in antenna arrays. In a dielectric substrate, the parasitic cross coupling is achieved by surface modes and further improved when high permittivity and thick substrate are utilized. As a result, electromagnetic band-gap (EBG) structures are formed to prevent the surface-waves propagation toward the next antenna at the bandgap frequencies [9], [13]-[14]. Changing the radiation pattern and the occupied space by EBG are major drawbacks of these structures. Defected ground structures (DGS) methods by means of various slots etched off metallic background to increase isolation were presented in [15] and [16]. The disadvantage of DGS is related to a backward signal leakage. Eigen-mode decomposition approach is utilized based on a 180° coupler [17]. Decoupling networks based on coupled resonators in array structures was studied [18]. These resonators are able to produce high-order resonance and broadband coupling reduction solution. However, both the Eigen-mode and decoupling network structures are inconvenient using complex structures [18]. In order to suppress the mutual coupling due to feed lines, the symmetric feeding network proposed in [19]. When the substrate with low permittivity is used, the dominant coupling is air coupling. Another approach for mutual coupling reduction using a coplanar strip wall between two antennas was reported in [20]. However, such a technique deteriorates the antenna's radiation pattern. This is because of the fact that the coplanar strip wall is not matched. Metamaterials have been widely analyzed in the recent years to improve many antenna radiation characteristics due to their unusual electromagnetic properties [21], [22]. In order to suppress the mutual coupling of the spatial electromagnetic fields, improving at the same time, the radiation performance of the antennas, metasurface, and frequency selective surface (FSS) as the superstrate of the antennas were proposed [6], [23]–[25]. Note that, depending on the antenna's radiation pattern shape, the spatially mutual coupling may be generated in either far or near-field areas. However, the decoupling designs operate on the basis of coupling reduction of either E or H-Fields between linearly polarized (LP) antennas. Recently, due to factors such as polarization mismatch, multipath phenomenon, and phasing subjects, the trend to design the circularly polarized (CP) antennas is expanding [26], [27]. As mentioned before, the most of the papers in the literature apply the similar principle to reduce the coupling among LP antennas. In [23], and [24] a new technique has been observed based on metasurface layer on the top of MIMO planar dipoles with the inter-element spacing 0.3λ and 0.5λ. However, it functions for linear structures and also the coupling reduction is not tangible, so that the improvement of 3dB and between 8 to 14 dB in different cases in the orientation of H-plane is obtained, whilst in the

E-plane coupling is not significant as compared with the air coupling (without superstrate).

In this paper, for the first time, coupling reduction behavior on MIMO-CP antenna systems based on a two-layer transmission-type FSS is investigated. Correspondingly, the FSS layers transmit the enormous portion of incident EM wave on the preferable frequency band. Therefore, the antenna's radiation pattern is slightly concentrated upward, ending up a spatially mutual coupling reduction between the antennas. However, due to this fact that each FSS element with different phases is illuminated, insignificant reflections are scattered from the FSS layers which is the main drawback of this approach. To solve this drawback, considering the FSS layers as a uniform planar array, the authors have determined the near-field behavior of FSS layers on the backside toward the radiating antennas. It is realized that by tuning few design parameters, the phase of reflections can be controlled. As a result, the insignificant reflections can easily be redirected along the nulls and away from the radiating antennas to prevent any interference. The paper is arranged as follows. The unit cell model of the FSS elements is detailed in Section II. The properties of a single-element aperture-coupled CP patch antenna are analyzed in Section III. Section IV is assigned to the structure of the MIMO-ACMA design and reflection array factor (AF) of the FSS layer in the nearfield region. The simulated results of the reflection coefficient, CP bandwidth, and influence of mutual coupling in a four-element array configuration (MIMO) with different inter-element spacing are determined in Section V. Next, the proposed structure is designed, fabricated, and the experimental results are presented in Section VI. Eventually, Section VII is dedicated to the conclusion.
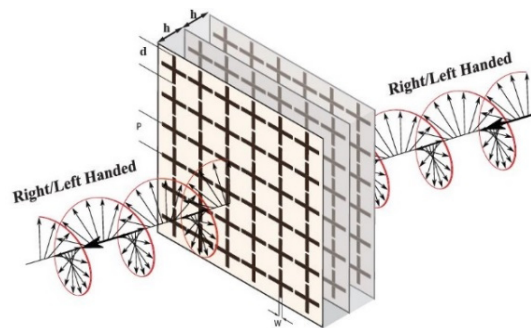


**FIGURE 1.** The schematic model of the transmission-type FSS superstrate illuminating by CP wave (h=0.787mm, d=2.7mm, P=3mm, and W=0.3mm)

## II. UNIT CELL MODEL OF FSS LAYERS

The transmission-type FSS layer topology is shown in Fig.1, where it consists of two identical dielectric boards, insulating Rogers 5880 with relative permittivity 2.2 and thickness 0.787mm, with the same cross dipole metal traces on each layer. The proposed FSS layer is able to transmit most of the CP incident wave within the desired frequency band without significant influence on its phase, magnitude and rotation
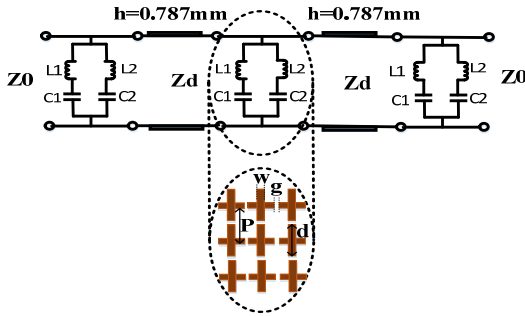
**FIGURE 2.** Equivalent circuit of FSS layer including inductive and capacitive elements [28], where ($z_d = \frac{z_0}{\sqrt{\varepsilon_r}}$).

orientation, as shown in Fig.1. Note that, in order to cover the broad bandwidth, the two dielectrics are attached to each other.

Fig.2 shows the equivalent circuit of FSS layer including inductive and capacitive elements, and transmission lines. The cross dipole traces can be separated into vertical and horizontal conducting strips and are modeled as inductive and capacitive elements, respectively. For an array of thin, continuous, infinitely long and perfectly conducting narrow strips, the shunt impedance is either inductive or capacitive, depending on the incident wave, whether it is polarized parallel to or perpendicular to the edge of the strips [28]. The vertical strips, parallel to electric field in the case of TE-wave, are modeled as a shunt inductive reactance in the equivalent circuit.

One should note that cross dipoles are symmetric in horizontal and vertical orientations. Also a CP wave is considered as a superposition of two orthogonal LP waves. Meanwhile, the equivalent circuit inductive reactance $F(P, W, \lambda)$ is given by [28]:

$$\frac{X_l}{Z_0} = \frac{d}{p} F(p, w, \lambda) \qquad (1)$$

$$B_g = 4 \frac{w}{p} F(p, w, \lambda) \qquad (2)$$

$$B_d = 4 \frac{d}{p} F(p, p - w, \lambda) \qquad (3)$$

Where different design parameters in (1)-(3) for the FSS unit cell of crossed dipole is exhibited in Fig. 3.
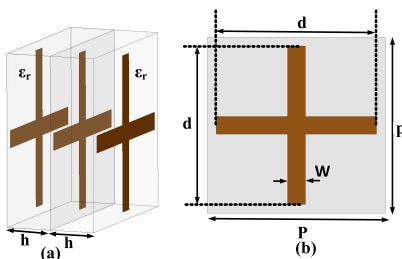


**FIGURE 3.** The unit cell model of crossed dipole FSS (a) side view and (b) top view (d=2.7mm, P=3mm, W=0.3mm and $\varepsilon$r=2.2, and h=0.787mm,).

It is observed that the same crossed dipole FSS traces are printed on the top, middle, and bottom of two substrate
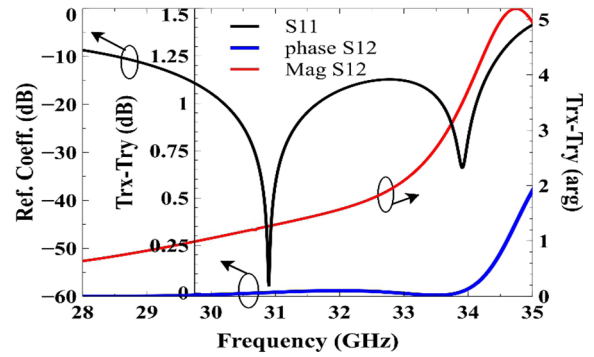


**FIGURE 4.** Simulated results of S-parameter for the unit cell model of FSS.

layers, Rogers 5880 with relative permittivity 2.2 and thickness 0.787mm. Once "P" is much lower than the wavelength, by the equivalent LC circuits in both directions of horizontal and vertical, not only the different resonances can easily be produced, but also the capability of phase control is yielded on the frequency band, contributing to a broader bandwidth. In order to observe the behavior of the crossed dipole FSS with infinite elements, the unit cell model of Ansys HFSS, which is a Finite-Element-Method (FEM) based on a full-wave simulator, is applied. In this model, two Floquet ports to excite along with master/slave boundaries are utilized. As shown in Fig. 4, the impedance bandwidth of the proposed design for $S_{11} \leq -10$dB is from 28.5GHz to 34.5 GHz (19%).

The transmission behavior of the crossed strip FSS elements can be determined by magnitude and phase of transmission coefficient. It is observed in Fig. 4 that on the impedance bandwidth (28.5-34.5GHz), amplitude and phase difference of two orthogonal transmitted field components for the incident CP wave is insignificant. As a result, the FSS layers nearly have an ideal transmission characteristic for the input CP wave.
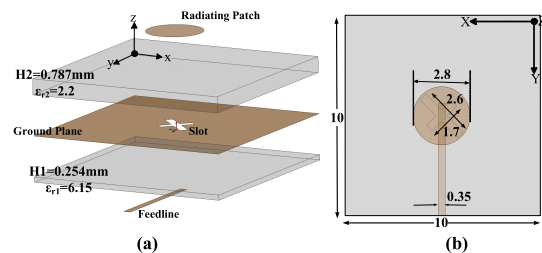


**FIGURE 5.** Geometry of single CP-ACMA (a) side view and (b) top view.

## III. SINGLE-ELEMENT ANTENNA DESIGN
In order to contribute to the wide frequency band and broadside pattern, a single aperture coupled microstrip antenna (ACMA) is presented. As depicted in Fig. 5, the ACMA with the capability of circular polarization consists of two different dielectrics as substrates: A Rogers 3006 ($\varepsilon_r = 6.15$, $H_1 = 0.254$mm) substrate on the bottom while the top one is Rogers 5880 ($\varepsilon_r = 2.2$, $H_2 = 0.787$mm).
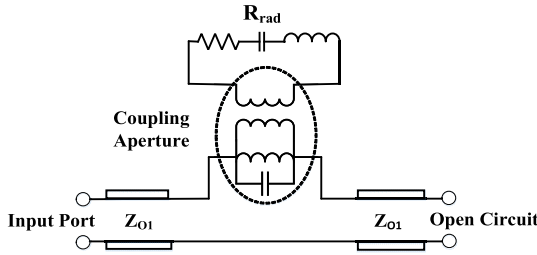
**FIGURE 6.** The equivalent circuit model of the ACMA [29].

On the middle of the ACMA, a conductive plate as a ground plane along with cross slot etched off its center is used to provide the required coupling. Besides, a 50-ohm microstrip feed line and a circle-shaped patch are printed on the lower and upper layers of the ACMA, respectively. The antenna is designed to operate at the center frequency 30GHz. Fig. 6 shows the equivalent circuit of the single ACMA. It consists of the input port and a quarter-wave impedance transformer from the center of the cross-shaped slot to the end of the line to represent the open circuit behavior. The simulated results of the reflection coefficient and axial ratio are shown in Fig. 7, in which exhibits that the ACMA covers impedance and CP bandwidths from 28GHz to 34GHz (19.3%) and 29.2GHz to 31GHz (6%), respectively.
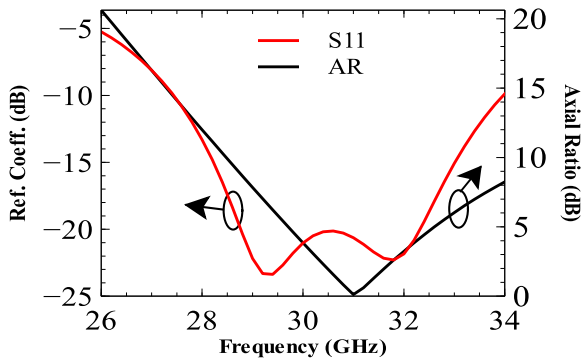


**FIGURE 7.** Reflection coefficient and axial ratio of a single element CP patch.

## IV. MIMO - ACMA DESIGN: REFLECTION ARRAY FACTOR

A Multiple-Input and Multiple-Output (MIMO) system is considered as a technique for multiplying the capacity of a radio link utilizing multiple transmit and receive antennas to exploit multipath propagation [30]. Using this concept, the proposed approach in this paper aims to determine the influence of the coupling between elements of the MIMO-ACMA. To achieve this goal, four elements of the ACMA are formed in two by two array to illuminate the FSS layers. The schematic diagram of the MIMO-ACMA is exhibited in Fig. 8, where the coupling coefficients in different directions and distance between the ACMAs are defined with parameters "$C_d$", "$C_v$", "$C_h$" and "di", respectively.

One of the main disadvantages of this approach is to scatter insignificant reflections from the FSS layers as compared with ones without FSS superstrate. These negligible
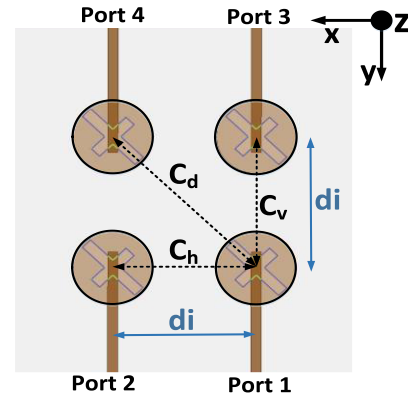


**FIGURE 8.** The schematic diagram of the MIMO-ACMAs with coupling coefficients ($C_d$, $C_h$, and $C_v$) and the inter-ACMA element spacing (di).
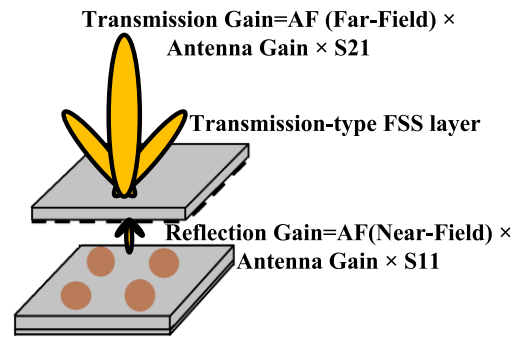


**FIGURE 9.** The schematic of the transmission-type FSS layer with transmission and reflection gains in two directions with respect to AF and S-parameters.

reflections occur due to the fact that the antenna sources illuminate the FSS elements with different oblique incidence angles. However, when the FSS elements are formed as a uniform planar array, it can deteriorate radiation levels of the antenna elements and degrades the mutual coupling between the radiating elements as well. Therefore, to overcome this problem, the reflection array factor (AF) in the near-field region is used. Since the array radiation pattern is always dominated by the AF, which has a scalar factor representing how the fields emitted from the many elements either in the near-field or far-field region. Therefore, the reflection effect is dominant when the number of FSS elements on the superstrates is increased. As shown in Fig. 9, the schematic of transmission-type FSS superstrate with transmission and reflection gains with respect to the S- parameters and AF is observed. It is apparent that the transmission gain at broadside is greater than reflected one at backside which demonstrates that the FSS layer is a transmission–type superstrate. As a result and as shown in Fig. 9, it is able to transmit a large proportion of the incidence wave and reflects a small part at the backside. In order to address the reflection drawback, some design parameters of the proposed structure should be tuned, so that the radiation pattern of the reflection AF be redirected along the radiation nulls of the external antenna sources. These design parameters prevent any interference
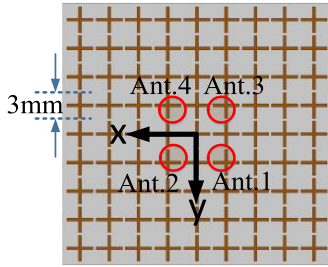
**FIGURE 10.** The formation schematic of FSS superstrate including 9×9 FSS elements, and the precise position of a 2×2 MIMO-ACMA below the superstrate in the x-y plane (the inter-element spacing $d_i = \lambda/2$).
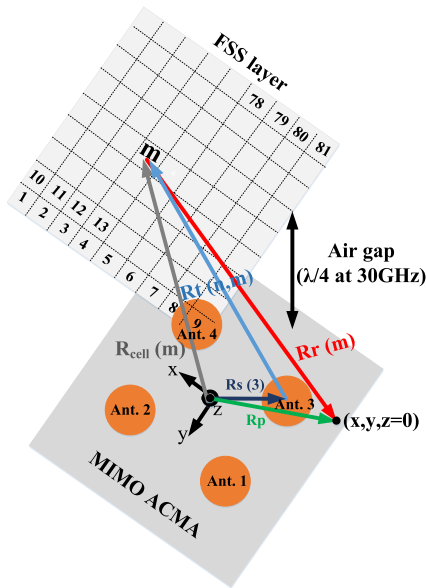


**FIGURE 11.** The sketch of a uniform rectangular array of 81 FSS elements with spacing 3mm along the x and y-axis above 2×2 MIMO-ACMA with an air gap 2.5mm along z-axis.

and deterioration in the radiation performance of external antenna sources.

To address the above issues, the near-field reflection array factor is investigated. Fig. 10 shows the sketch of 9×9 FSS elements on the superstrate along with the 2×2 MIMO ACMA below the FSS superstrate. The FSS array to be considered is uniform and planar in the x-y plane, as shown in Fig. 10. The air gap between the external antenna sources and FSS layer is 2.5mm ($\lambda_0/4$ at 30GHz). Therefore, the induced current amplitude on each FSS element is assumed to be identical and isotropic.

Therefore, to formulate the array factor, the phases of FSS elements' excitation currents when illuminated by a 2×2 MIMO antenna system should be computed. Fig. 11 shows the geometry of a uniform planar array including 81 FSS elements above 2×2 MIMO-ACMA system with an air gap $\lambda/4$ at 30GHz (2.5mm) to compute the AF in the near-field region. Each FSS element occupies an identical area of $3\times3$mm² on the x-y plane. Referring to Fig. 11, $R_s(n)$ represents the
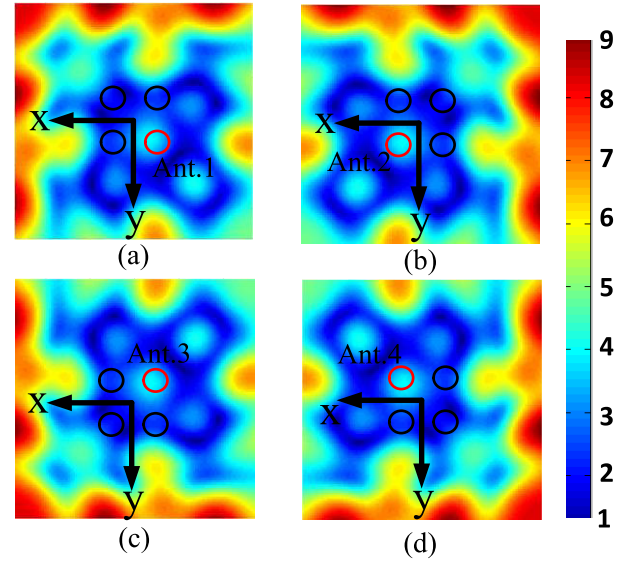


**FIGURE 12.** The 2-D reflection power density of the FSS elements on the antenna plane (the x- and y-axis) when those are illuminated separately by (a) Ant. 1, (b) Ant. 2, (c) Ant. 3, and (d) Ant. 4.

location of each antenna element, n=1, 2, 3, 4, and the center position of the FSS unit cell is given by $R_{cell}(m)$, where m=1, 2, 3, ..., 81. Therefore, the electric field at the center of the $m^{th}$ FSS unit cell when illuminated by the $n^{th}$ antenna element can be calculated as

$$\overrightarrow{E_t}(n, m) = E_0(e^{-\alpha R_t(n,m)} \times e^{-j\beta R_t(n,m)})\widehat{a_r} \quad (4)$$

Where

$$R_t(n, m) = R_{cell}(m) - R_s(n) \quad (5)$$

and $\alpha$ is the propagation loss in the air gap, and it is negligible and almost zero, and $\beta$ is the corresponding propagation phase. In addition, $E_0$ is the magnitude of electric field which is assumed to be a constant. Thus, it can be simplified as

$$\overrightarrow{E_t}(n, m) = E_0 e^{-j\beta R_t(n,m)} \quad (6)$$

Meanwhile, $R_p$ and $R_r(m)$ can be defined as

$$R_p = x\widehat{a_x} + y\widehat{a_y} \quad (7)$$

$$R_r(m) = R_p + R_{cell}(m) \quad (8)$$

When the $n^{th}$ antenna element is illuminating the FSS layer, the reflected electric field at point (x, y, z=0) can be calculated as

$$\overrightarrow{E_r}(x, y, z = 0, n) = E_0 \sum_{m=1}^{81} \Gamma(n, m) \times e^{-j\beta R_t(n,m)}$$
$$\times e^{-j\beta R_r(m)}\widehat{a_r} \quad (9)$$

where $\Gamma(n, m)$ is the reflection coefficient at the center of the $m^{th}$ unit cell, when the wave is radiated by the $n^{th}$ antenna element. Note that, $\Gamma(n, m)$ is calculated using the unit cell simulation model by Ansys HFSS, as shown in Fig. 4. The antenna has circular polarization, so the vector $\widehat{a_r}$ in (4) is rotating with an angular speed of $\omega_o = 2\pi f_o$, where $f_o$ is
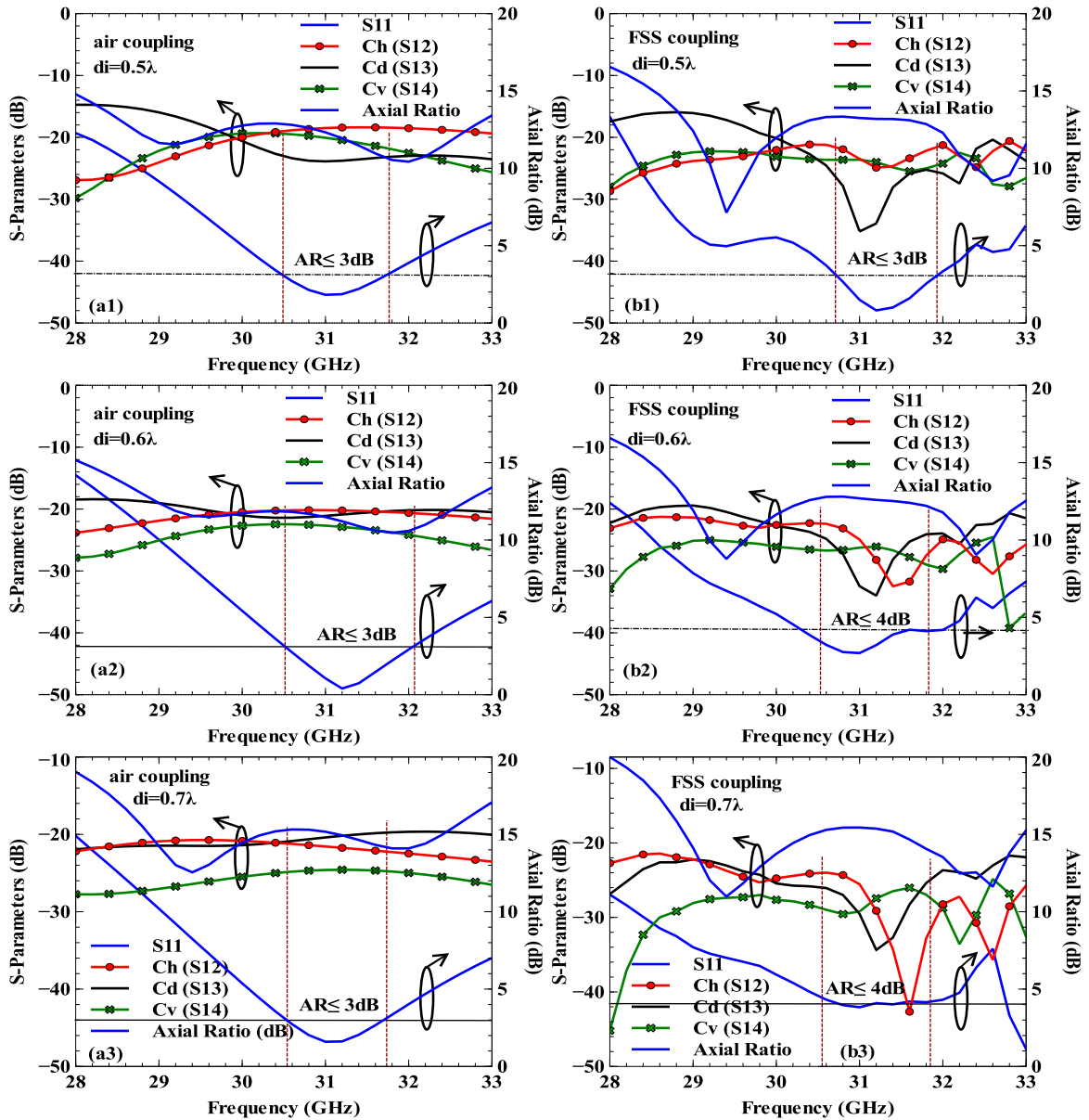
**FIGURE 13.** Simulated results of axial ratio and S-parameters for different cases of (a) Air coupling and (b) FSS coupling; including (a1) and (b1) (di = 0.5λ), (a2) and (b2) (di = 0.6λ), and (c1) and (c2) (di = 0.7λ).

wave frequency. Since CP wave is considered as superposition of two orthogonal LP waves, therefore, the normalized reflection power density at a point (x, y, z=0) when the $n^{th}$ antenna is radiating can be calculated as

$$\left| \overrightarrow{E}_r \left(x, y, z = 0, n\right) \right| = \sum_{m=1}^{81} \Gamma(n, m) \times e^{-j\beta R_t(n,m)}$$
$$\times e^{-j\beta R_r(m)} \quad (10)$$

Fig. 12 shows the simulated 2D normalized reflection power density at z=0, when individual antenna elements is radiating. As a result, it is observed that the air gap between FSS superstrate and the antenna plane is considered as a key design parameter. For the proposed structure, the air gap with

value 2.5mm (λ/4 at 30GHz) is a reasonable choice to redirect the reflection power density away from the MIMO-ACMA in order to prevent interference and deterioration in the antenna radiation characteristics.

## V. SIMULATED RESULTS OF THE MIMO-ACMAs

In this section, the simulated results of 2×2 MIMO-ACMA for air and FSS couplings using the full-wave simulator Ansys HFSS are presented. One should note that in order to prevent enlarging the structure size and redirect reflected power density away from the MIMO antennas, the air gap between ACMA elements and FSS layer is considered to
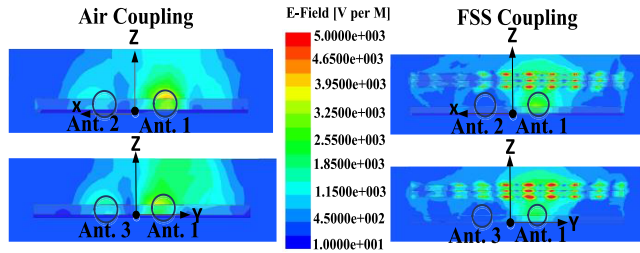
**FIGURE 14.** Simulated E-Field distribution on the 2 × 2 MIMO-ACMA for both cases air and FSS couplings in the xz- and yz- planes at frequency 31.2GHz.
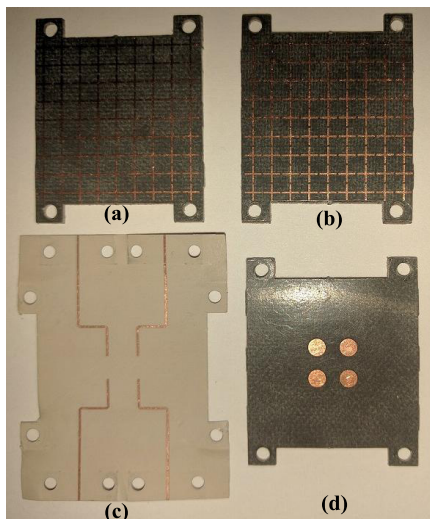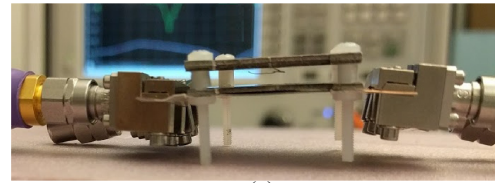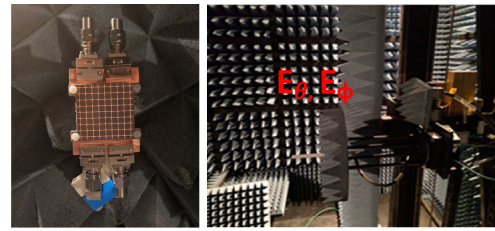


**FIGURE 15.** Photos of the fabricated 2×2 MIMO-ACMA: (a) and (b) FSS layers, (c) feedlines, and (d) patches.



(c)

**FIGURE 16.** (a) The photography of the fabricated 2×2 CP-MIMO antennas under test as transmitter, (b) the photo of open ended waveguide (NSI RF WR28) as receiver in the far-field anechoic chamber, and (c) side view of the proposed 2×2 MIMO-ACMA under test by network analyzer.

**TABLE 1.** The maximum coupling coefficients on cp bandwidth

| $d_i$ | Without superstrate (air coupling) (dB) | With superstrate (FSS Coupling) (dB) | |
|---|---|---|---|
| $0.5\lambda$ | $C_h=16$ $C_v=18$ $C_d=24$ | $C_h=24$ $C_v=24$ $C_d=36$ | (AR≤3dB) |
| $0.6\lambda$ | $C_h=20$ $C_v=24$ $C_d=20$ | $C_h=32$ $C_v=27$ $C_d=34$ | (AR≤4dB) |
| $0.7\lambda$ | $C_h=23$ $C_v=25$ $C_d=20$ | $C_h=43$ $C_v=30$ $C_d=34$ | (AR≤4dB) |

be 2.5mm (λ/4 at 30GHz). The simulated results of the axial ratio and S-parameters of the proposed structure for the two cases of air and FSS couplings, when the inter-element spacing varies from 0.5λ to 0.7λ, are presented in Fig. 13. It is observed that the impedance bandwidth (s11≤ −10dB) for all cases is nearly identical, covering a band from 28GHz to 33GHz (16.4%). Therefore, it is noticed that the inter-element spacing and FSS layer do not significantly affect the impedance characteristics. On the other hand, the axial ratio is determined when the inter-element spacing is changed for the two cases of air and FSS couplings. It is seen that in the case of air coupling by varying antenna distance from 0.5λ to 0.7λ, the axial ratio magnitude has a negligible change without any frequency shift. However, the axial ratio is degraded in terms of magnitude and frequency shift when FSS layer is employed. It is believed that the air gap (2.5mm) between FSS element and MIMO antenna changes the phase of two electric field components ($E_\theta$, $E_\emptyset$) which is given as [26], [27];

$$AR\,(dB) = 10Log(\frac{\left|\left|\overrightarrow{E_\theta} + j\overrightarrow{E_\emptyset}\right| + \left|\overrightarrow{E_\theta} - j\overrightarrow{E_\emptyset}\right|\right|}{\left|\left|\overrightarrow{E_\theta} + j\overrightarrow{E_\emptyset}\right| - \left|\overrightarrow{E_\theta} - j\overrightarrow{E_\emptyset}\right|\right|}) \quad (11)$$

Thus, in order to satisfy the requirement of the 3dB-axial ratio in the case of FSS coupling, the inter-element spacing 0.5λ has an acceptable response as compared with 0.6λ and 0.7λ spacing as shown in Fig. 13 (a2)-(c2). It is worthwhile to mention that coupling reduction is higher when the inter-element spacing is considered 0.7λ in comparison to the other 0.5λ and 0.6λ spacing. However, the priority here is to maintain the 3dB-AR bandwidth and then coupling reduction. Table 1 summarizes the maximum coupling coefficients in the two cases of air and FSS couplings for different inter-element spacing values on the CP bandwidth. As it is apparent, in spite of the further coupling suppression when the antenna distance is 0.7λ or 0.6λ, the CP bandwidth does not meet the AR≤3dB. Consequently, in order to satisfy the AR≤3dB, the inter-antenna spacing 0.5λ is considered for the implementation.

The simulated electric field distribution for two cases of air and FSS couplings at 31.2GHz using Ansys HFSS is shown in Fig. 14. Note that the reason to select 31.2GHz is that the best value of the axial ratio for both cases is obtained at that frequency. It can be found out that in the case of FSS coupling, the field leakage through adjacent antennas in the
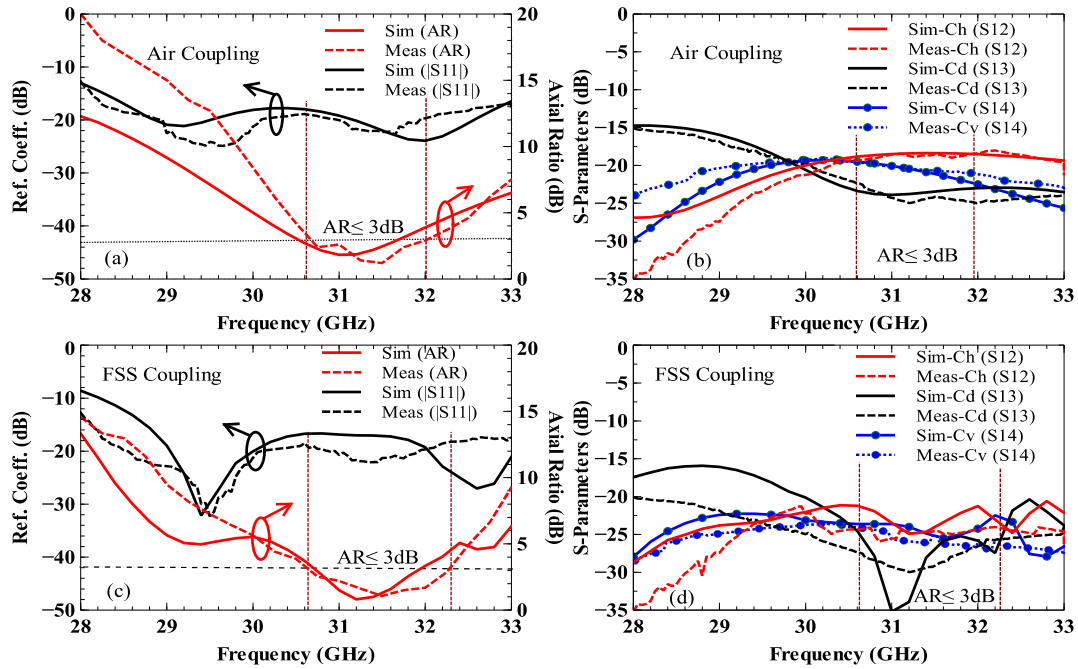
**FIGURE 17.** Measured and simulated results of axial ratio, reflection coefficient for different cases of (a) air and (c) FSS couplings, along with measured and simulated results of coupling for different cases of (b) air and (d) FSS couplings.

xz- and yz- planes is less than the one in the case of air coupling.

## VI. FABRICATION AND MEASUREMENTS

Finally, the proposed 2×2 MIMO-ACMA system with the inter-antenna spacing λ/2 for both cases of air and FSS coupling are fabricated and measured. The photographs of the implemented 2×2 MIMO-ACMA are shown in Fig. 15. For the sake of comparison, the coupling coefficients without and with the FSS layers were measured. The coupling between 2×2 MIMO-ACMA is measured with a two port Agilent N5227A PNA Network Analyzer (10MHz-67GHz). For all structures, the coupling amounts are achieved by normalizing the experimental results with the radiated power [23]. Thus, the coupling coefficient can be expressed as [23]:

$$C\,(dB) = 10\log\left(\frac{|S_{21}|^2}{\left(1-|S_{11}|^2\right)\left(1-|S_{22}|^2\right)}\right) \qquad (12)$$

Using (12) and the measured s-parameters, the coupling coefficients "$C_h$", "$C_v$", and "$C_d$" can be computed.

The photography of the implemented structure and also the measurement setup are observed in Fig. 16(a) and (b). A side view of the configuration is shown in Fig. 16(c). It should be noted that the simulated results for the coupling coefficients $S_{21}$, $S_{31}$, and $S_{41}$, are computed directly using HFSS without applying (12). Fig. 17 shows the simulated and experimental s-parameters and axial ratio for the proposed design for the two cases of air and FSS couplings. The measurements show an acceptable agreement with simulations. The highest values of measured coupling coefficients for the proposed structure in the absence and presence of

**TABLE 2.** The maximum amount of measured coupling coefficients on CP bandwidth.

| Without superstrate (air coupling) (dB) | With superstrate (FSS Coupling) (dB) |
|---|---|
| $C_h$ = -18 | $C_h$ = -25 |
| $C_v$ = -20 | $C_v$ = -26 |
| $C_d$ = -24 | $C_d$= -31 |

the FSS superstrate on the CP bandwidth in three directions of horizontal, vertical, and diagonal are also summarized in Table 2.

The same conclusion as before can be reached with the presence of FSS superstrate. The isolation improvement in the diagonal direction is better than the ones in other directions. In addition, the coupling reduction in the horizontal and vertical directions approximately is the same. Fig. 18 shows the effect of mutual coupling on the radiation performance of ACMA. The left-hand circularly polarized (LHCP) gain in the xz- and yz- planes were simulated using HFSS. The radiated patterns are also measured in the presence and absence the FSS superstrate at frequency 31GHz. As shown in Fig. 18(a) and (b), when the ACMA elements are radiating in free space at 31 GHz, the radiation pattern is slightly tilted due to the spatially mutual coupling and the presence of the common ground plane. Assuming that Ant.1 is radiating (see Fig. 10), the positions of Ant.2 and 3 with respect to Ant.1 are $\theta = 90°$ in the x-z plane and $\theta = -90°$ in the y-z plane, respectively.

With the presence of FSS layers, radiation pattern in the yz-plane at $\theta = -90\circ$ (Fig. 18(c)), is reduced nearly
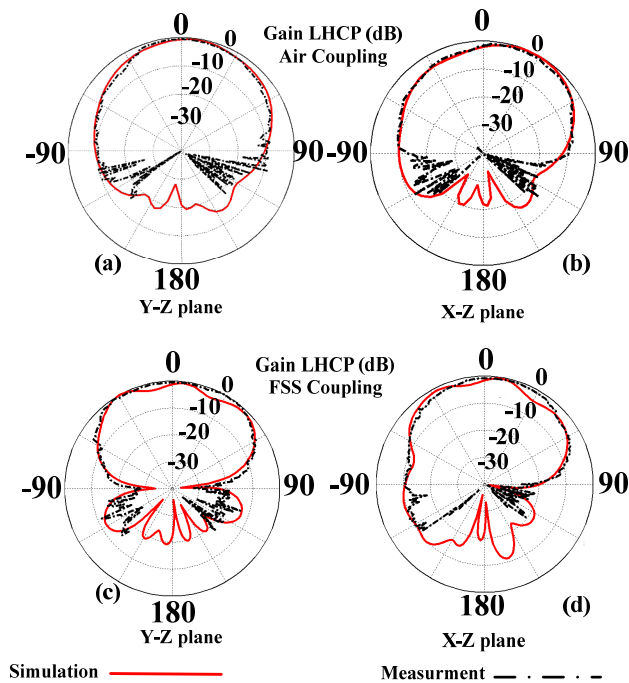
**FIGURE 18.** Measured and simulated LHCP gain for both cases of (a), (b) air coupling and (c), (d) FSS coupling in the yz- and xz- planes at frequency 31 GHz.

by 20 dB as compared with it in the case of air coupling (Fig. 18(a)). Therefore, it can be concluded that coupling Ch between adjacent Ant. 1 and 2 has been suppressed. On the other hand, coupling Cv between Ant. 1 and Ant. 3 can be determined such that with adding FSS layers, the radiation pattern in the xz-plane shown in Fig. 18(d) at $\theta = 90°$ sees a reduction of approximately 10 dB by itself as compared with it in the case of air coupling shown in Fig. 18(b). In the same manner, it can be found out that coupling Cv between adjacent Ant. 1 and 3 has been mitigated. Note that, since the coupling reduction in the proposed structure occurs in the near-field region, thus, it cannot accurately predict same coupling reduction with respect to the LHCP gain in Far-field. In addition, the reason for the 10° tilting in radiation pattern can be attributed to the design of FSS unit cell element under normal incident waves, while in the proposed integrated structure it is illuminated at oblique angles as shown in Fig. 10. Furthermore, using FSS superstrate, the radiation pattern is slightly concentrated upward in the broadside direction, improving the antenna gain by about 1.5 dB such that the FSS superstrate acted as a dielectric lens [26].

## VII. CONCLUSION

In this paper, an effective method for suppressing the near-field coupling between $2 \times 2$ CP-MIMO antennas around 30 GHz has been presented. The suppression has been achieved by incorporating a two-layer transmission-type FSS superstrate. Due to the concentration of the power density using the FSS superstrate, enhancement in the structure gain

and improvement in isolation have been achieved. The main disadvantage of this method is the partial reflection of power density from the FSS elements because the antenna illuminates each FSS element in different oblique incidence angles. The FSS unit cells are considered as a uniform planar array scattering back a small portion of the power density through the radiating antennas. In order to address this disadvantage, the reflected power density in the near-field area, when the FSS elements are illuminated by the antennas, has been studied. It is found out that by adjusting few design parameters such as the inter-antenna spacing or air gap, the insignificant reflections can be redirected far from the main beam direction to prevent any interference. However, by varying the air gap spacing, the CP bandwidth may be slightly varied due to variations in the phases of the electric field components ($E_\theta$, $E_\emptyset$). The study has also compared the mutual coupling between CP-MIMO antennas when the patches are radiating in air and in the presence of the FSS layers. In order to validate the simulation results, the proposed structures with an inter-antenna spacing of 0.5λ have been implemented and measured. The measured results indicate when the FSS layers are employed, an average coupling suppression of 6 to 7 dB on the 3dB-AR bandwidth has been achieved.

## REFERENCES

[1] H. S. Farahani, M. Veysi, M. Kamyab, and A. Tadjalli, "Mutual coupling reduction in patch antenna arrays using a UC-EBG superstrate," *IEEE Antennas Wireless Propag. Lett.*, vol. 9, pp. 57–59, Jan. 2010.

[2] G. Dubost, "Influence of surface wave upon efficiency and mutual coupling between rectangular microstrip antennas," in *Antennas Propag. Soc. Int. Symp. Dig.*, vol. 2, Dallas, TX, USA, May 1990, pp. 660–663.

[3] P. R. Haddad and D. M. Pozar, "Anomalous mutual coupling between microstrip antennas," *IEEE Trans. Antennas Propag.*, vol. 42, no. 11, pp. 1545–1549, Nov. 1994.

[4] M. A. Khayat, J. T. Williams, D. R. Jackson, and S. A. Long, "Mutual coupling between reduced surface-wave microstrip antennas," *IEEE Trans. Antennas Propag.*, vol. 48, no. 10, pp. 1581–1593, Oct. 2000.

[5] R. L. Xia, S. W. Qu, P. F. Li, Q. Jiang, and Z. P. Nie, "An efficient decoupling feeding network for microstrip antenna array," *IEEE Antennas Wireless Propag. Lett.*, vol. 14, pp. 871–874, 2015.

[6] B. C. Pan *et al.*, "Reduction of the spatially mutual coupling between dual-polarized patch antennas using coupled metamaterial slabs," *Sci. Rep.*, vol. 6, Jul. 2016, Art. no. 30288.

[7] T. S. Rappaport *et al.*, "Millimeter wave mobile communications for 5G cellular: It will work!," *IEEE Access*, vol. 1, pp. 335–349, May 2013.

[8] J. R. Costa, E. B. Lima, C. R. Medeiros, and C. A. Fernandes, "Evaluation of a new wideband slot array for MIMO performance enhancement in indoor WLANs," *IEEE Trans. Antennas Propag.*, vol. 59, no. 4, pp. 1200–1206, Apr. 2011.

[9] M. J. Al-Hasan, T. A. Denidni, and A. R. Sebak, "Millimeter-wave compact EBG structure for mutual coupling reduction applications," *IEEE Trans. Antennas Propag.*, vol. 63, no. 2, pp. 823–828, Feb. 2015.

[10] H. M. Bernety and A. B. Yakovlev, "Reduction of mutual coupling between neighboring strip dipole antennas using confocal elliptical metasurface cloaks," *IEEE Trans. Antennas Propag.*, vol. 63, no. 4, pp. 1554–1563, Apr. 2015.

[11] C.-H. Wu, C.-L. Chiu, and T.-G. Ma, "Very compact fully lumped decoupling network for a coupled two-element array," *IEEE Antennas Wireless Propag. Lett.*, vol. 15, pp. 158–161, 2016.

[12] S. C. Chen, Y. S. Wang, and S. J. Chung, "A decoupling technique for increasing the port isolation between two strongly coupled antennas," *IEEE Trans. Antennas Propag.*, vol. 56, no. 12, pp. 3650–3658, Dec. 2008.

[13] R. Gonzalo, P. de Maagt, and M. Sorolla, "Enhanced patch-antenna performance by suppressing surface waves using photonic-bandgap substrates," *IEEE Trans. Microw. Theory Techn.*, vol. 47, no. 11, pp. 2131–2138, Nov. 1999.

[14] I. Ederra et al., "A 250 GHz subharmonic mixer design using EBG technology," *IEEE Trans. Antennas Propag.*, vol. 55, no. 11, pp. 2974–2982, Nov. 2007.

[15] D. Guha, S. Biswas, M. Biswas, J. Y. Siddiqui, and Y. M. M. Antar, "Concentric ring-shaped defected ground structures for microstrip applications," *IEEE Antennas Wireless Propag. Lett.*, vol. 5, no. 1, pp. 402–405, Dec. 2006.

[16] F.-G. Zhu, J.-D. Xu, and Q. Xu, "Reduction of mutual coupling between closely-packed antenna elements using defected ground structure," *Electron. Lett.*, vol. 45, no. 12, pp. 601–602, 2009.

[17] S. Zuo, Y.-Z. Yin, Z.-Y. Zhang, W.-J. Wu, and J.-J. Xie, "Eigenmode decoupling for MIMO loop-antenna based on 180° coupler," *Prog. Electromagn. Res. Lett.*, vol. 26, pp. 11–20, Aug. 2011.

[18] L. Zhao, L. K. Yeung, and K.-L. Wu, "A coupled resonator decoupling network for two-element compact antenna arrays in mobile terminals," *IEEE Trans. Antennas Propag.*, vol. 62, no. 5, pp. 2767–2776, May 2014.

[19] C. Oikonomopoulos-Zachos, "Double layer compact four-port antenna using a symmetrical feeding technique for future MIMO antenna systems at 5.6 GHz," in *Proc. IEEE Antennas Propag. Soc. Int. Symp.*, Toronto, ON, Canada, Jul. 2010, pp. 1–4.

[20] H. Qi, L. Liu, X. Yin, H. Zhao, and W. J. Kulesza, "Mutual coupling suppression between two closely spaced microstrip antennas with an asymmetrical coplanar strip wall," *IEEE Antennas Wireless Propag. Lett.*, vol. 15, pp. 191–194, 2016.

[21] T. Negishi, D. Erricolo, and P. L. E. Uslenghi, "Metamaterial spheroidal cavity to enhance dipole radiation," *IEEE Trans. Antennas Propag.*, vol. 63, no. 6, pp. 2802–2807, Jun. 2015.

[22] A. Mehdipour, T. A. Denidni, and A.-R. Sebak, "Multi-band miniaturized antenna loaded by ZOR and CSRR metamaterial structures with monopolar radiation pattern," *IEEE Trans. Antennas Propag.*, vol. 62, no. 2, pp. 555–562, Feb. 2014.

[23] E. Saenz, I. Ederra, R. Gonzalo, S. Pivnenko, O. Breinbjerg, and P. D. Maagt, "Coupling reduction between dipole antenna elements by using a planar meta-surface," *IEEE Trans. Antennas Propag.*, vol. 57, no. 2, pp. 383–394, Feb. 2009.

[24] E. Saenz, K. Guven, E. Ozbay, I. Ederra, and R. Gonzalo, "Decoupling of multifrequency dipole antenna arrays for microwave imaging applications," *Int. J. Antennas Propag.*, vol. 2010, Mar. 2010, Art. no. 843624.

[25] M. Ghaderi and N. C. Karmakar, "Frequency selective surface for reducing mutual coupling in antenna arrays," in *Proc. Asia–Pacific Microw. Conf. (APMC)*, Melbourne, VIC, Australia, 2011, pp. 1877–1880.

[26] M. Akbari, S. Gupta, M. Farahani, A. R. Sebak, and T. A. Denidni, "Gain enhancement of circularly polarized dielectric resonator antenna based on FSS superstrate for MMW applications," *IEEE Trans. Antennas Propag.*, vol. 64, no. 12, pp. 5542–5546, Dec. 2016.

[27] M. Akbari, S. Gupta, M. Farahani, A. R. Sebak, and T. A. Denidni, "Analytic study on CP enhancement of millimeter wave DR and patch subarray antennas," *Int. J. RF Microw. Comput.-Aided Eng.*, vol. 27, no. 1, p. e21053, Jan. 2017.

[28] D. Singh, A. Kumar, S. Meena, and V. Agarwala, "Analysis of frequency selective surfaces for radar absorbing materials," *Prog. Electromagn. Res. B*, vol. 38, pp. 297–314, Feb. 2012.

[29] A. Pirhadi, H. Bahrami, and J. Nasri, "Wideband high directive aperture coupled microstrip antenna design by using a FSS superstrate layer," *IEEE Trans. Antennas Propag.*, vol. 60, no. 4, pp. 2101–2106, Apr. 2012.

[30] H. Lipfert, "MIMO OFDM (space time coding-spatial multiplexing increasing performance and spectral efficiency in wireless systems)," Institut Fur Rundfunktechnik, Munich, Germany, Tech. Rep., Aug. 2007.

**MOHAMMAD AKBARI** (S'15) received the B.Sc. degree in engineering-telecommunication from the University of Shahid Bahonar, Kerman, Iran, in 2007, and the M.Sc. degree in electrical engineering-telecommunication from the University of Urmia, Urmia, Iran, in 2011. He is currently pursuing the Ph.D. degree at Concordia University, Montréal, QC, Canada. He has taught courses in microwave engineering, antenna theory, fields and waves, and electromagnetics. He has authored or co-authored approximately 60 peer-reviewed scientific journals and international conference papers. His main field of research focuses on analysis and design of microstrip antennas, modeling of microwave structures, electromagnetic theory and analysis of UWB antennas for WBAN applications, antenna interactions with human body, mm-wave technology, phased and switched-beam arrays, microstrip antennas and circuits, sequential feedings, periodic structures and their application to antenna design and performance enhancement. He was a recipient of the Graduate Concordia Merit Scholarship.

**HAMDAN ABO GHALYON** (S'16) received the B.Sc. degree in communications engineering technology from Al-Balqa' Applied University, Amman, Jordan, in 2009, and the M.Sc. degree in electrical and computer engineering from the New York Institute of Technology, NY, USA, in 2010. He is currently pursuing the Ph.D. degree at the Electrical and Computer Engineering Department, Concordia University, Montréal, QC, Canada, where he is involved in research activities. His main current research interests include millimeter-wave high-gain antennas, beamforming techniques, FSS, metamaterials, DRA, and polarization converters.

**MOHAMMADMAHDI FARAHANI** (S'17) received the Diploma degree in electrical engineering and applied electromagnetism engineering from the Iran University of Science and Technology, Tehran, Iran, in 2012. He is currently pursuing the Ph.D. degree with the Institut National de la Recherche Scientifique, Universite de Quebec, Montréal, QC, Canada. He was a Researcher with the IUST Antennas and Microwave Research Laboratory, RF Communications Systems Group, from 2009 to 2012. His current research interests include phase array antennas, adaptive arrays, switched multibeam antenna arrays, FSS structures, dielectric resonator antennas, metamaterial antennas, and microwave components development for wireless communications systems.

**ABDEL-RAZIK SEBAK** (F'10) received the B.Sc. degree (Hons.) in electrical engineering from Cairo University, Cairo, Egypt, in 1976, the B.Sc. degree in applied mathematics from Ein Shams University, Cairo, in 1978, and the M.Eng. and Ph.D. degrees in electrical engineering from the University of Manitoba, Winnipeg, MB, Canada, in 1982 and 1984, respectively. From 1984 to 1986, he was with Canadian Marconi Company, where he was involved in the design of microstrip phased array antennas. From 1987 to 2002, he was a Professor with the Department of Electronics and Communication Engineering, University of Manitoba. He is currently a Professor with the Department of Electrical and Computer Engineering, Concordia University, Montréal, QC, Canada. His research interests include phased array antennas, millimeter-wave antennas and imaging, computational electromagnetics, and interaction of EM waves with engineered materials, and bio electromagnetics. He was the Technical Program Co-Chair for the 2015 IEEE ICUWB Conference. He is a member of the Canadian National Committee of International Union of Radio Science Commission B. He was a recipient of the 1992 and 2000 University of Manitoba Merit Award for outstanding Teaching and Research, the 1994 Rh Award for Outstanding Contributions to Scholarship and Research, and the 1996 Faculty of Engineering Superior. He has served as the Chair of the IEEE Canada Awards and Recognition Committee from 2002 to 2004 and the Technical Program Chair of the 2002 IEEE CCECE Conference and the 2006 URSIANTEM Symposium.

**TAYEB A. DENIDNI** (M'98–SM'04) received the M.Sc. and Ph.D. degrees in electrical engineering from Laval University, Quebec, QC, Canada, in 1990 and 1994, respectively. He was a Professor with the Engineering Department, Université du Quebec in Rimouski, Rimouski, QC, Canada, from 1994 to 2000, where he founded the Telecommunications Laboratory. Since 2000, he has been with the Institut National de la Recherche Scientifique (INRS), Université du Quebec, Montréal, QC, Canada. He found the RF Laboratory with INRS-EM, Montréal. He has extensive experience in antenna design and is leading a large research group consisting of three research scientists, eight Ph.D. students, and two M.Sc. students. His current research interests include reconfigurable antennas using EBG and FSS struc tures, dielectric resonator antennas, metamaterial antennas, adaptive arrays, switched multibeam antenna arrays, ultrawideband antennas, microwave, and development for wireless communications systems. He served as an associate editor of the IEEE TRANSACTIONS ON ANTENNAS and PROPAGATION from 2008 to 2010. From 2005 to 2007, he served as an associate editor of the IEEE ANTENNAS WIRELESS PROPAGATION LETTERS. Since 2015, he has been an associate editor of *IET Electronics Letters*.

● ● ●